# Thermally resistant geopolymer to 1300 °C: Scale-up and structural evolution

Lila Ouamara, Ameni Gharzouni, Benoit Naït-Ali, Jouin Jenny, Guillaume Babule, Patrice Duport, Clifford Chinaya, Eric Guillaume, Sylvie Rossignol

Open Ceramics 16 (2023) 100462

Contents lists available at ScienceDirect

Open Ceramics

journal homepage: www.sciencedirect.com/journal/open-ceramics

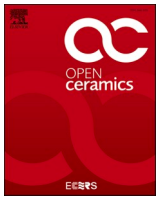

# Thermally resistant geopolymer to 1300 °C: Scale-up and structural evolution

Ouamara Lila [a], Gharzouni Ameni [a], Naït-Ali Benoit [a], Jouin Jenny [a], Babule Guillaume [a], Duport Patrice [a], Chinaya Clifford [b], Guillaume Eric [b], Sylvie Rossignol [a,*]

[a] Institut de Recherche sur les Céramiques (IRCER), 12 rue Atlantis, 87068, Limoges Cedex, France
[b] Efectis France, Voie Romaine 57280 Maizières-lès-Metz, France

ARTICLE INFO

Handling Editor: Dr P Colombo

*Keywords:*
Geopolymer
Fire resistance
Scale up
Fire protection

ABSTRACT

Geopolymers are promising ecofriendly materials for temperature-resistant applications. For this purpose, the synthesis of thermally resistant, alkali-activated binders based on metakaolin with additives (silica sand, calcite and mullite) has been studied. In this work, the stabilities of the mechanical and thermal properties of geopolymer binders based on metakaolin with additives during scale transfer are investigated. The geopolymer is prepared by mixing metakaolin, silica sand, calcite and mullite with two different alkaline silicate solutions. The scale-up process does not affect the processing conditions. After the temperature tests at the laboratory and pilot scales (two ramps selected 200 and 400 °C/min) the same phases crystallized (leucite, wollastonite and kalsilite), and the microstructure (viscous flow formation) is the same, thus confirming the scalability of the formulation. These different results show that these formulations displaying a value of 50 MPa and $\lambda = 1.45$ W m$^{-1}$ K$^{-1}$, are promising for fire protection and fire resistance applications.

## 1. Introduction

The evolution of road traffic and new construction due to economic prosperity requires the development of new materials to prevent fire risks. Fire is a highly severe condition that structures can be subjected to; therefore, the use of fire-resistant materials is crucial. New materials, such as geopolymers, address this issue due to their excellent fire resistance properties such as refractory materials [1]. Tognonvi et al. [2] studied the fire resistance properties of geopolymer binders based on a mixture of kaolin and Callovo–Oxfordian argilite calcined at two different temperatures. Researchers have demonstrated that the material they studied possesses either the ability to maintain or enhance its mechanical strength after treatment at 1000 °C. Beyond this temperature, however, the samples have shown numerous cracks and low resistance. Moreover, Petlitckaia et al. [3] focused on the effects of consolidation time and water immersion of geopolymers on their thermal behaviors. Another works mentioned the effect of tubular halloysite [4], the use of zeolite [5] or of foam additive to enhance thermal resistant of geopolymer [6]. The statement suggested that the age of consolidation had no impact on the mechanical strength of geopolymer materials, both before and after undergoing thermal treatment. To improve the thermal behavior and resistance, a modification of the formulation is necessary. Rashad et al. [7] have shown that modifying the composition by adding sand or filler induces a strong increase in the mechanical properties at high temperatures, and it can reduce the total shrinkage at 1000 °C. The addition of several mineral sources to the base composition contributes to the structure of the material at high temperatures [8,9]. In previous work, Dupuy et al. [10] have shown that the use of calcite during heat treatment induces the formation of wollastonite, resulting in mechanical and thermal strengthening. The use of sand is known to enhance working properties such as mechanical properties [11]. Even, to enhance mechanical and thermal properties, the addition of mullite is used in the manufacture of refractory products, to improve mechanical and thermal performance at temperature above 1300 °C [12] Indeed, during geopolymer treatments at different temperatures, crystallization is generally observed. Scanferla et al. [8] demonstrated that geopolymers with low potassium concentrations have better mechanical resistance levels than geopolymers with high potassium concentrations; at high potassium concentrations, the geopolymers experience the formation of different geopolymer networks that form either leucite and wollastonite phases or only a kalsilite phase. Duxson et al. [13] and Kohout et al. [14] have stated that the formation

* Corresponding author.
*E-mail address:* sylvie.rossignol@unilim.fr (S. Rossignol).

https://doi.org/10.1016/j.oceram.2023.100462
Received 16 June 2023; Received in revised form 7 September 2023; Accepted 7 September 2023
Available online 9 September 2023

**Table 1**
Data on solid and liquid precursors.

| Name | Acronym | Supplier | Characteristic | Chemical composition |
|---|---|---|---|---|
| **Potassium silicate solution** | $K^5$ | Wollener | d = 1.415 | Si/M = 0.5, [K] = 5.0 mol/L |
| | $K^6$ | | d = 1.358 | Si/M = 0.8, [K] = 5.3 mol/L |
| **Metakaolin** | M | Argeco | $D_{50}$ = 42 μm | SiO2 : 60.0/Al2O3 : 35.3 |
| **Blansil** | S | Sibelco | $D_{50}$ = 210 μm | SiO2 : 99.0 |
| **Sablon** | | Argeco | $D_{50}$ = 190 μm | SiO2 : 95.6/ CaCO3 : 4.6 |
| **Calcite** | | Ceradel | $D_{50}$ = 3 μm | $CaCO_3$ = 98.0 |
| **Mullite** | A | Nabaltec | $D_{50}$ = 30 μm | SiO2 : 26/Al2O3 : 72 |

temperatures of leucite and kalsilite phases depend on the K/Al ratio. Christopoulou et al. [15] observed that kalsilite is an unstable phase that behaves as an intermediate precursor to leucite. Consequently, at high temperatures, the formation of leucite, kalsilite and wollastonite is strongly dependent on the chemical composition and formed networks.

Few works have developed data concerning the scale transfer of geopolymers. The three-dimensional (3D) manufacturing of geopolymers is possible by controlling the formulation and robotization processes [16]. La Scalia et al. [17] explained that the change in scale from laboratory to industry implies a change in the process, especially for the different stages of product development. Indeed, during industrialization, it is possible to reduce the duration of some steps, such as drying, and to introduce intermediate steps, such as the preparation of raw materials. It is important to select the type of equipment used, such as tanks with highly alkaline liquids [18]. Scaling up is possible, but attention must be paid to processes that undergo process change and adaptation. The objective of this study is to prove the scale transfer of laboratory geopolymer samples based on a mixture of metakaolin, sand and additives with two alkali silicate solutions. First, the feasibility and characterization of laboratory samples at various temperatures is investigated by determining mechanical strength under compression, X-ray diffraction and dilatometry. Then, a pilot test is performed with different-sized samples to compare their thermal behaviors and microstructures. Finally, a comparison of both tests is performed by X-ray diffraction (XRD) and scanning electron microscopy (SEM) observations.

## 2. Experiment

### 2.1. Raw materials and sample preparation

The samples were prepared using an aluminosilicate source, additives and two different alkaline silicate solutions (Table 1). The aluminosilicate source was metakaolin, which was supplied by Argeco; laboratory samples were characterized based on their temperature. Two potassium alkaline solutions with Si/K molar ratios of 0.58 and 0.80 were used [19], and they were supplied by Wollner. Then, silica sand (sablon and blansil), calcite and an aluminosilicate additive (mullite) were added to the binder by following the procedure described in previous works [20] (Fig. 1A). The weight percentages of sand, calcite, and mullite, referred to as metakaolin mass, in the various formulations were 60, 14, and 26%, respectively. The nomenclature used to identify the geopolymer samples was $K^X$MSA, where x = 5 or 6 refers to alkaline solution, $K^5$ = 0.80, $K^6$ = 0.58, M refers to metakaolin, S refers to quartz sand and calcite, and A refers to mullite, the aluminosilicate additive. Samples with dimensions of 100 × 100 $mm^2$ and thicknesses of 20 mm (200000 $mm^3$) were prepared. The dimensions of the samples and the weight factor are within the limits for laboratory use. These initial dimensions were multiplied by 50 and 120 to obtain samples with dimensions of 500 × 500 $mm^2$ and 1200 × 500 $mm^2$, with thicknesses of 40 mm. To achieve a change in scale, different volumes of mixer were used (1 and 100 L). The obtained mixture was cast in a closed mold and stored at room temperature for two days.

### 2.2. Characterization techniques

The compressive strength was determined using an Instron 5969 instrument equipped with a 50 KN load cell and Bluehill3 software. The samples were cylindrical in shape with diameters of 15 mm and heights of approximately 30 mm. For repeatability of measurements, the tests were performed on five specimens after 3 and 7 days of endogenous consolidation.

Uniaxial compression tests were performed on cylindrical samples with an aspect ratio of 2 (Ø = 15 mm, h = 30 mm) after 7 days at room temperature and after heating at 1000 °C. An Instron 5969 with a load cell of 50 kN and a crosshead speed of 0.5 mm/min was used. The maximum compressive strength $\sigma_{max}$ was calculated from the average values seven samples for each treatment composition and temperature.

XRD patterns were obtained with a D8 diffractometer (Brucker)

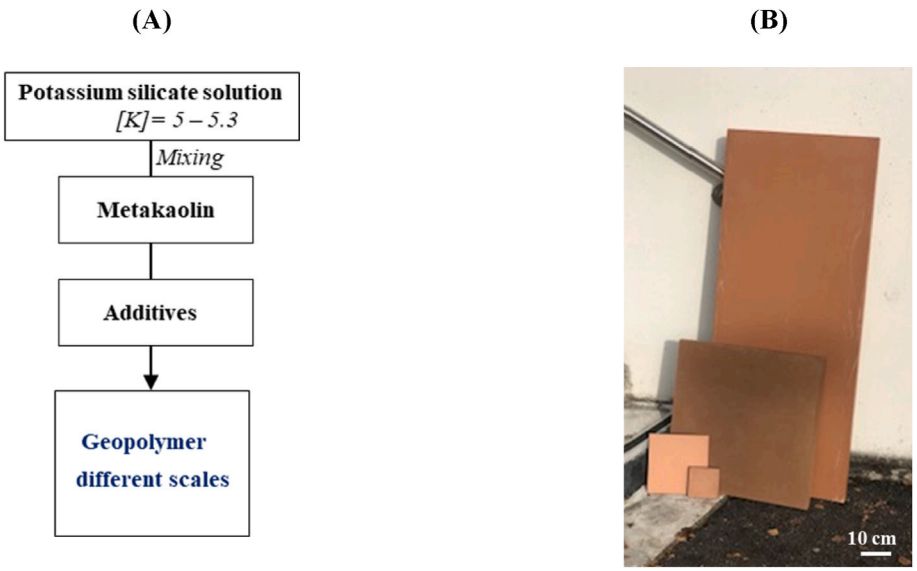


**Fig. 1.** (A)Protocol of the preparation of the geopolymer samples and (B) photo of the geopolymer samples at different sclaes

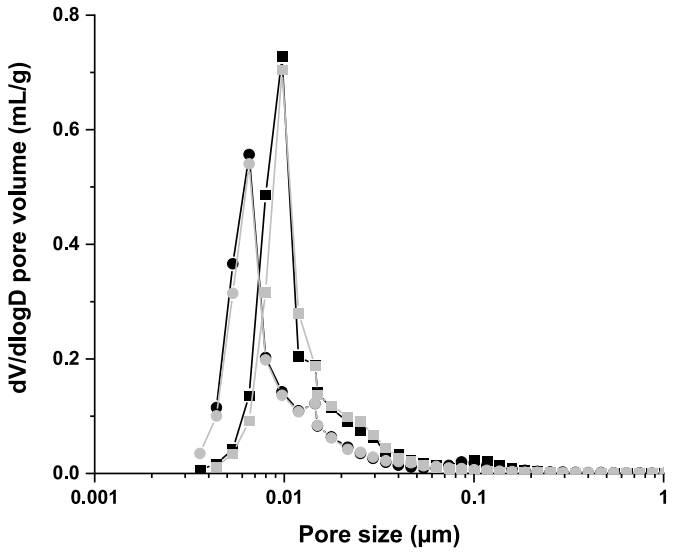


**Fig. 2.** Values of the (dV/dlogD) pore volume as a function of the pore size for (■) $K^6$MS (●) $K^5$MS, (▰) $K^6$MSA and (◍) $K^5$MSA samples.

equipped with a Bragg–Brentano mount. XRD is based on the interaction between an X-ray beam and a material. Calcined powder samples were analyzed over a range of 5–50° (2θ) with a step time of 1 s. The identification of the crystalline phases was performed with EVA software using powder diffraction file (PDF) reference sheets.

Mercury intrusion porosimetry tests (MIP) were conducted using a Micromeritics Autopore IV 9510 porosimeter that could detect pore diameters varying between 450 µm and 3 nm. The mercury pressure gradually increased from 0.2 to 400 MPa. Tests were performed in two steps: (1) low-pressure step to remove gases, fill the samples with mercury and test at a pressure of 345 kPa and (2) high-pressure step with a pressure that could reach a pressure of 400 MPa.

Dilatometric measurements were performed in air with a vertical dilatometer Setsys made by Setaram Instrumentation. The cylindrical samples (6-mm heights and 5-mm diameters) were placed between two platinum/alumina holders during the analysis, and a correction was applied to remove the contributions of the device/holders. Samples were heated to 1200 °C at 20 °C/min.

The thermal conductivities of the samples were measured using the transient plane source technique with a Hot Disk Transient Plane Source (TPS) 1500 supplied by Hot Disk AB (Sweden) [21]. The radius of the probe and the measuring time were 6.403 mm and 80 s, respectively.

The microstructural analysis was conducted using an FEI Quanta 450 Field Emission Gun (FEG) microscope (SEM). The preparation process consisted of fixing the samples on a sample holder with a carbon pad without metallization.

Efectis (Maizières-lès-Metz laboratory) supplier was chosen to determine the temperature resistance levels of the large samples (1200 × 500 $mm^2$) by following the standard International Organization for Standardization (ISO) 834 fire curve for the first step and the hydrocarbon major (HCM) curve for the second step. The temperature rise was controlled semiautomatically by the following equations: $T = 345 \log_{10}(8t+1) + 20$ and $T = 1280 (1–0.325\, e^{-0.167t}–0.675\, e^{-2.5t}) + 20$ (where t = time (min) and T = temperature at time t (°C)) for steps 1 and 2, respectively. The furnace temperature was measured by plate pyrometers, as defined in the standard EN 1363–1. The samples were horizontally placed and simply supported to have an exposure length of 1000 mm. Thermocouples and displacement gauges were placed on the samples to monitor temperature and deflection.

**Table 2**
Values of compressive strength and density of samples treated at room temperature.

| Composition | σ (MPa) ±2 | Density (g/$cm^3$) | Porosity (%) |
|---|---|---|---|
| **$K^6$MS** | 36 | 1.935 | 33 |
| **$K^6$MSA** | 40 | 1.984 | 31 |
| **$K^5$MS** | 52 | 1.963 | 29 |
| **$K^5$MSA** | 52 | 1.993 | 27 |

## 3. Results

### 3.1. Laboratory-scale geopolymers at 25 °C

Fig. 2 shows the variations in the pore sizes for the four samples determined by mercury intrusion, and the porosity values are shown in Table 2. $K^6$MS displays a pore size distribution centered on 0.01 µm with a broadened evolution to mesopores; for the samples based on $K^5$, the main pore sizes are centered on nanopores and some micropores. This behavior involves a decrease in porosity from 33% to 29% for the $K^6$MS and $K^5$MS samples. The decrease in porosity by adding fillers occurs due to the optimization of the granular skeleton, which is optimal [22] since particles do not contribute to the reaction; instead, they allow better packing by filling the structural pores [23]. Arnoutl et al. [24] demonstrated by Raman spectroscopy of different silicate solutions that a high log value for rings and chains is linked to a high reactivity. Scanferla et al. [25] show that $K^6$ is a more reactive solution with a ring-to-chain ratio of 1.01, which accelerates the kinetic reaction, increases the structure porosity, and increases the pore sizes on the consolidated material. However, $K^5$ is a solution with a high condensation degree, and the obtained geopolymers react relatively slow, resulting in a sample with relatively low porosity [26].

Compressive strength tests and the density at 7 days of the different samples treated at room temperature are determined and shown in Table 2 and Fig. 3. For the $K^6$MS sample, the curve obtained is characterized by a fragile rupture of the geopolymer [27,28] with a value of 36 MPa (1.935 g/$cm^3$) (Table 2). The addition of mullite ($K^6$MSA) induces a slight increase in the mechanical strength (40 MPa) and density (1.984 g/$cm^3$). The change in solution ($K^5$MS and $K^5$MSA) induces an increase in the mechanical strength (52 MPa). The data agree with the improved mechanical properties of the $K^5$-based samples [25]. The difference can be explained by the reactivity levels of the solutions.

In this work, $K^5$ displays more condensed Si species than $K^6$. This difference enhances the mechanical properties since the network is more polymerized.

### 3.2. Structural and mechanical evolution from 25 to 1300 °C

To evaluate the thermal resistance from room temperature to 1300 °C, Table 3 presents pictures of samples $K^5$MS and $K^6$MS. All the samples display good features regardless of the selected temperature. The changes in color from red to white to gray occur due to the iron species from the hematite in the metakaolin [29] being responsible for the initial red color. In fact, during thermal treatment, the iron species could react either to form ferrosilicate species as mentioned by Nodari et al. [30] or trapped in viscous flow [31,32]. In our sample, ferrosilicate species could not detected due to a low amount or not formed.

To understand structural evolution as a function of temperature, X-ray diffraction data are gathered and displayed in Fig. 4 for the $K^6$MS sample treated at different temperatures (25–1300 °C). The results of the $K^5$ samples are reported in the supplementary file. At 25 °C, the diffractogram presents kaolinite and calcite, as evidenced in previous work [33]. The increase in the temperature at 1000 °C induces the formation of kalsilite, leucite and wollastonite. At higher temperatures (1100 °C), the same peaks are present, and the intensity of kalsilite decreases. However, leucite and wollastonite increase. At a temperature of

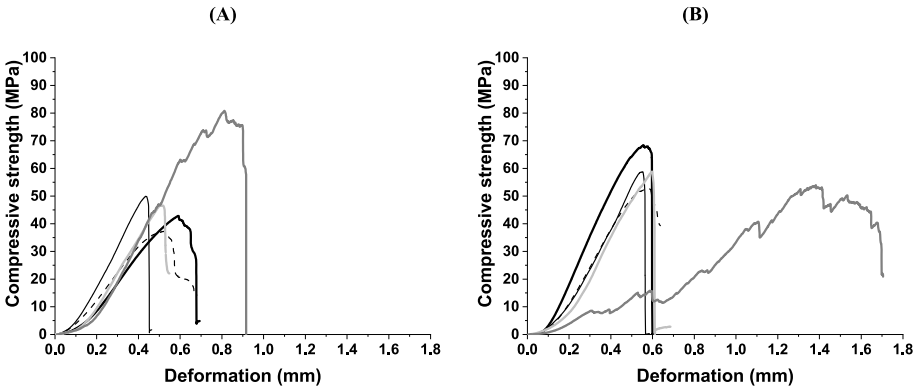


**Fig. 3.** Evolution of compressive strength as a function of the deformation for (A) $K^6MS$ and (B) $K^5MS$ samples treated at (■) 25, (■) 500, (–) 1000, (■) 1100 and (■) 1300 °C.

**Table 3**
Appearance of the samples after the thermal treatment. At different temperature.

| Composition | Temperature (°C) 25 | 500 | 1000 | 1100 | 1300 |
|---|---|---|---|---|---|
| $K^6MS$ |  |  |  |  |  |
| $K^5MS$ |  |  |  |  |  |

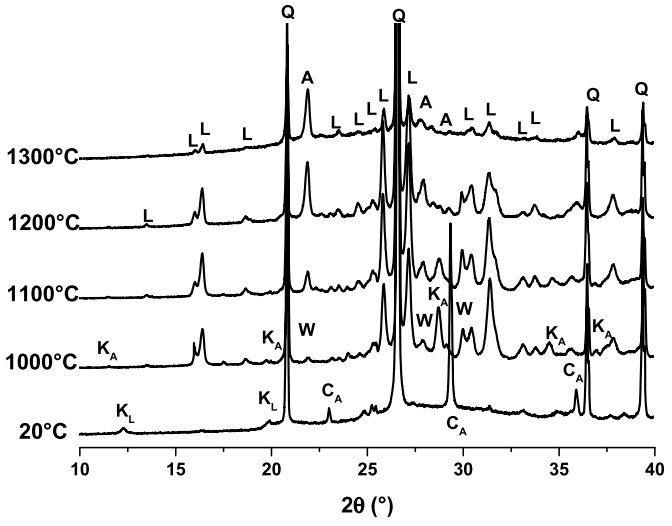


**Fig. 4.** X-ray pattern of $K^6MS$ sample treated at different temperature (PDF files: quartz (Q) 01-089-1961, calcite (CA) 00-005-0586, kaolinite (KL) 00-001-0527; kalsilite (KA) 00-002-0297, leucite (L) 01-076-8732, wollastonite (W) 00-002-0629_00-005-0586 and anorthite (A) 04-011-1371).

**Table 4**
Main contribution of X-ray for samples based on the $K^6$ or $K^5$ solution treated at different temperature.

| Composition | Température (°C) 1000 | 1100 | 1200 | 1300 |
|---|---|---|---|---|
| $K^6$ | $K_A$, L, W | $K_A$, L, W | L, A | L, A |
| $K^5$ | L, W | L, W | L, A | L, A |

(PDF files: kalsilite (KA) 00-002-0297, leucite (L) 01-076-8732, wollastonite (W) 00-002-0629_00-005-0586 and anorthite (A) 04-011-1371).

1200 °C, kalsilite and wollastonite are not detected, leucite is present, and the appearance of another phase is observed (anorthite) [34]. After the thermal treatment at 1300 °C, only leucite and anorthite are present. Table 4 presents a comparison of the phases in the two different solutions $K^6$ and $K^5$ at different temperatures. Solutions $K^6$ and $K^5$ have Si/K ratios of 0.58 and 0.80, respectively. For samples containing the $K^6$ solution, only kalsilite, leucite and wollastonite are noted at 1000 °C. The same phases are present when the sample is treated at 1100 °C. At 1200 and 1300 °C, only leucite and anorthite are detected. Relative to the sample treated with $K^5$ solution, the same phases are present at the same temperatures without kalsilite, which agrees with the work of Scanferla et al. [8]. All phases are responsible for the thermal resistance. To correlate the structural evolutions of samples, the intensity ratios of the

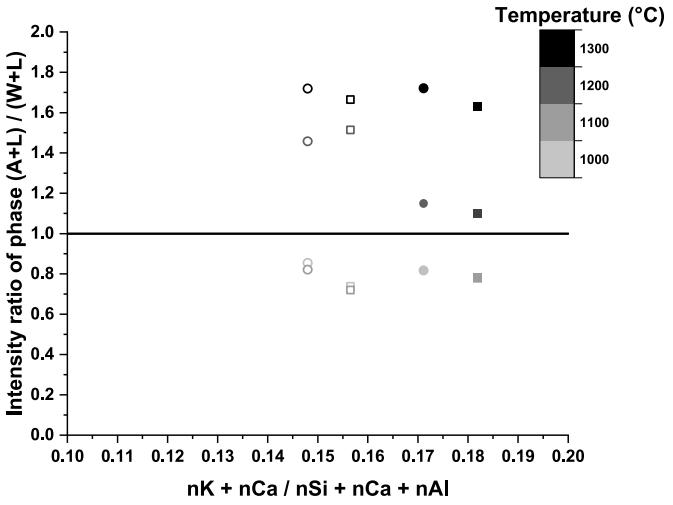


**Fig. 5.** Evolution of intensity ration of phase as a function of the K + Ca/Si + Ca + Al molar ratio for (■) K6MS, ▱ K6MSA, (●) K5MS, and (◯)K5MSA samples at different temperature.

phases (anorthite + leucite)/(wollastonite + leucite) ((A + L)/(W + L)) as the temperature changes are plotted based on the molar ratios of the (K + Ca) cations to the (Si + Ca + Al) cations in the mixtures (Fig. 5). At 1000 and 1100 °C, all samples show the same behaviors, with intensity ratios less than 1 due to the absence of anorthite. A slight difference is observed with the change in solution. At these temperatures, only leucite and wollastonite phases are formed. Beyond 1200 °C, a change is observed, and the intensity ratio (A + L)/(W + L) exceeds 1 for all samples. This phenomenon can be explained by the formation of the new anorthite phase and the decomposition of the wollastonite phase. The reference samples $K^6$MS and $K^5$MS show relatively low intensity ratios because of the reduced availability levels of Al and Si in the geopolymer.

The addition of mullite enriches the network in Si and Al, which increases the intensity ratio and promotes the formation of the anorthite phase (Equation (1)).

$$6CaSiO_3 + 2(3Al_2O_3)\cdot 3(2SiO_2) \rightarrow 6CaAl_2Si_2O_8 \quad \text{Eq. 1}$$

At 1300 °C, species diffusion is important, increasing the availability of Si and Al species to form more anorthite for all samples. The chemical composition controls the formed phases during treatment at different temperatures. This control induces an increase in mechanical strengths with increasing temperature.

To complete these data, dilatometric measurements are performed for the $K^6$MS and $K^5$MS samples in Fig. 6A. The dilatometric curves present the same dimensional variations until 800 °C. The first variation, below 300 °C, occurs due to the loss of the water in the poral network; the second variation, at 600 °C, occurs due to the phase transition of quartz in α–β. Above 700 °C, several shrinkages are observed. For the $K^6$MS sample, from 800 to 1000 °C, the greatest shrinkage is observed, which occurs due to the formation of a viscous flow. Then, from 1000 to 1150 °C, a delay in shrinkage is observed, which occurs due to the crystallization of leucite and kalsilite [35]. Above 1150 °C, the same behavior is visible due to the crystallization of anorthite. For the $K^5$MS sample, only two shrinkages are detected. The formation of viscous flow occurs at a higher temperature (998 °C) than $K^6$MS (976 °C) during the first shrinkage. Above 1060 °C, a delay in shrinkage is observed due to the crystallization of leucite and anorthite. This difference is induced by the change in solution, as observed by Scanferla et al. [25]. To correlate the thermal properties to the chemical composition mixtures, the first shrinkage is plotted as a function of the molar ratio Si/K in the mixtures (Fig. 6B). The temperature increases with increasing ratio, depending on the alkaline solutions and aluminosilicate sources. Samples based on $K^6$ exhibit lower viscous flow formation temperatures than samples based on $K^5$. The geopolymer network is more favorable with samples based on $K^5$ than $K^6$. The addition of the aluminosilicate additive enriches the network in $SiO_2$, increasing the ratio and delaying the formation temperature of viscous flow [36].

Compressive strength tests are performed at 7 days on several compositions ($K^6$MS and $K^5$MS) treated at different temperatures (500, 1000, 1100 and 1300 °C), and the curves are reported in Fig. 3. For the

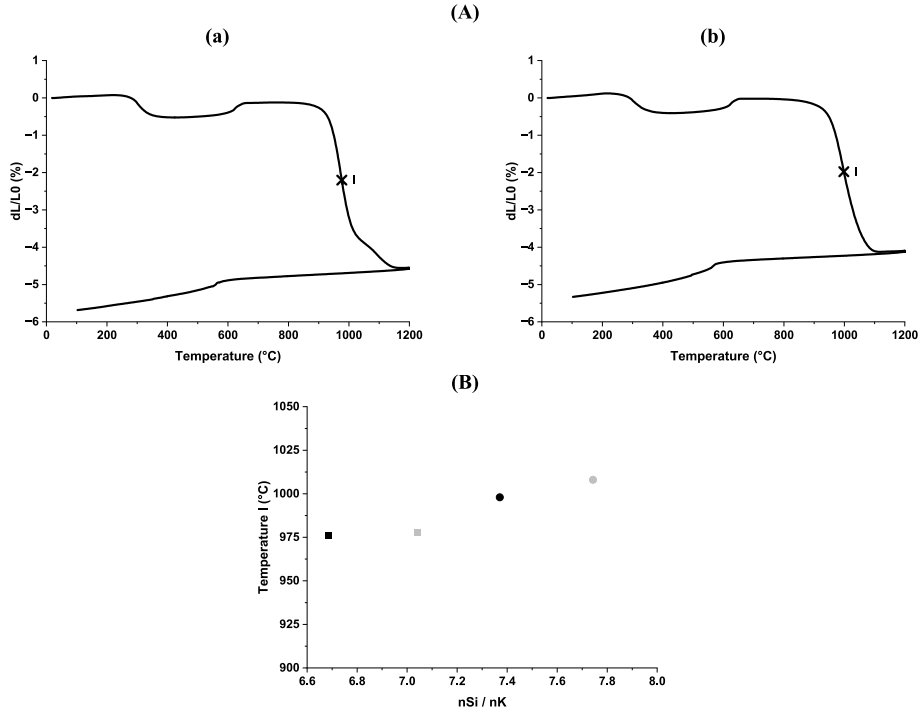


**Fig. 6.** (A) Dilatometric curves of (a) $K^6$MS and (b) $K^5$MS samples and (B) evolution of the temperature I according to Si/K molar ratio for (■) $K^6$MS, (◯) $K^6$MSA, (●) $K^5$MS, and (◍)$K^5$MSA samples.

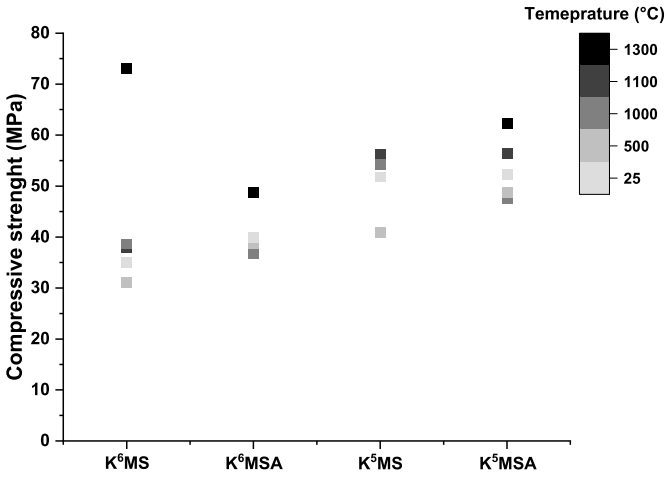


**Fig. 7.** Evolution of compressive strength as function of the samples treated at different temperature.

$K^6$MS sample, between 500 °C and 1100 °C, brittle fracture is observed [28]. At 1300 °C, a behavior similar to that of a composite is observed, with a significantly increased deformation value. This increase in mechanical properties can be induced by the formation of certain crystalline phases, such as anorthite, in materials. Changing the solution involves some differences in the mechanical behavior at varying temperatures. The use of $K^5$ solution induces the same behavior regardless of the treatment temperature, except for the sample treated at 1300 °C. Characteristic brittle failure of ceramics and maintenance of the compressive strength are observed at temperatures of 500, 1000 and 1100 °C. At 1300 °C, the composite exhibits a significant decrease in mechanical strength. The evolution characteristics of the compressive strengths at different temperatures for $K^6$MS, $K^6$MSA, $K^5$MS and $K^5$MSA are presented in Fig. 7. For the $K^6$MS sample, with a value of 35 MPa at 20 °C, the increase in temperature induces little change in mechanical strength values between 500 and 1100 °C. This change can be induced by the formation of viscous flow, as observed by Duxon et al. [37]. However, at 1300 °C, a change is observed with a significant increase in the mechanical strength from 36 to 73 MPa [27]. The addition of mullite ($K^6$MSA) allows a slight increase in the mechanical strengths relative to the reference, but the same behavior is observed at varying temperatures. However, the $K^5$MS sample at room temperature has a relatively large mechanical strength (52 MPa). Therefore, increasing the thermal treatment temperature improves the mechanical properties. The additive does not affect the mechanical properties.

### 3.3. *Scale-up and normalized thermal resistance test (ISO 834 and HCM)*

To verify the shaping feasibility, the compositions $K^6$MS, $K^6$MSA and $K^5$MSA are cast in different-sized molds and shaped by casting to form plates of different shapes. A photo of the shape is displayed in Fig. 1B. 100x100 × 20 $mm^3$ plates are the first sample made, then 200x200 × 20 $mm^3$ is used for the laboratory test. For large samples, the volume varies from 0.01 to 0.024 $m^3$. The change in scale does not induce any change in the preparation and final appearance of the sample. In advance, it is

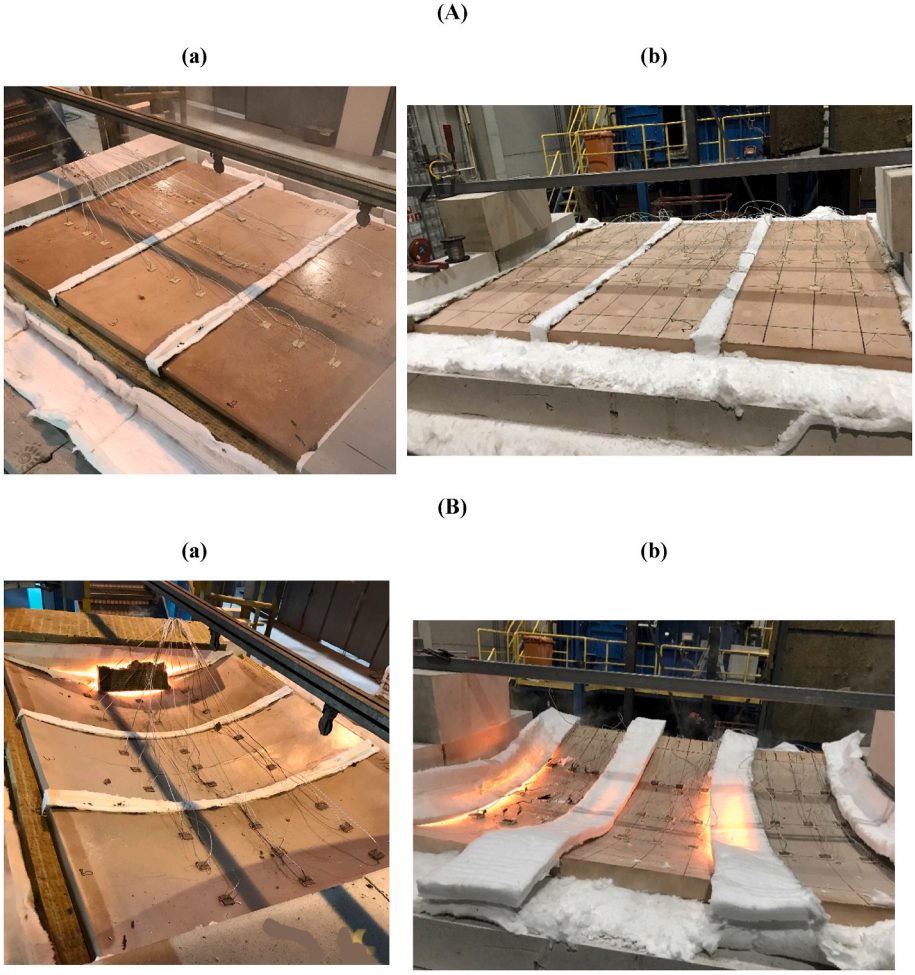


**Fig. 8.** photos of the samples (A) before and (B) after the thermal treatment using (a) the ISO 834-1 standard thermal program and (b) the HCM thermal program.

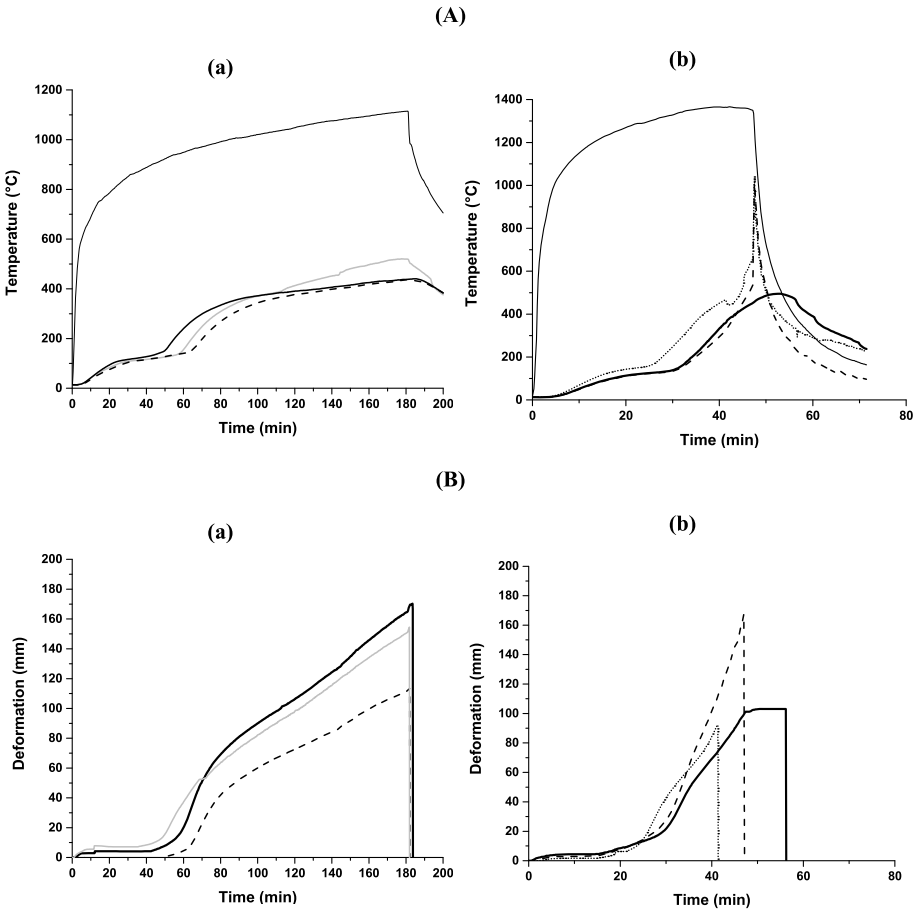


**Fig. 9.** Evolution of the (A) temperature and (B) deformation as function of the time during the ISO 834-1 standard thermal program (a) and the HCM thermal program (b) for (■, ▬) $K^6MS$, (▬▬) $K^6MSA$ and (····) $K^5MSA$ composition.

important to determine the properties of the material, starting with characterizing the samples at the laboratory scale.

To validate the results observed in the laboratory, large-scale tests of thermal resistance are performed on different geopolymer compositions ($K^6MS$, $K^6MSA$ and $K^5MSA$) to simulate various fire conditions, and two types of tests with different temperature ramps are performed. Fig. 8 shows the visual aspects of the samples before and during the large-scale heat treatment in steps 1 and 2 of the test. At the beginning of the tests, the samples are placed horizontally on the furnace with a fire exposure distance of 1000 mm. During step 1, between 100 and 200 °C, color modification of the samples induced by the departure of water is observed, which agrees with the work of Jiang et al. [38]. Longitudinal cracks appear on the samples, which show creep over time. After 180 min, all samples show excellent thermal resistance. In step 2, the samples undergo significant thermal shocks that induce creep after 47 min of exposure. The evolution characteristics of temperature and deformation over time are plotted in Fig. 9 for clarification. During step 1, a gradual increase in furnace temperature to 1000 °C is observed. For all samples, a temperature plateau below 200 °C is observed for 60 min; then, an increase occurs before the temperature stabilizes below 400 °C. The increase in the ramp speed (step 2) reduces the duration of the first step to 30 min, but a limitation of heat transfer is observed and maintained at a maximum of 400 °C when the oven temperature exceeds 1200 °C. For compositions $K^6MSA$ and $K^5MSA$, a peak in temperature is observed at 1000 °C because the samples break and the thermocouples are directly exposed to the heat of the oven. These results affirm that geopolymers are comparable to refractories due to their fire protection (low thermal conduction) and fire resistance (low deformation) properties [23]. In addition, two compositions are tested ($K^6MS$ and $K^6MSA$) during step 1.

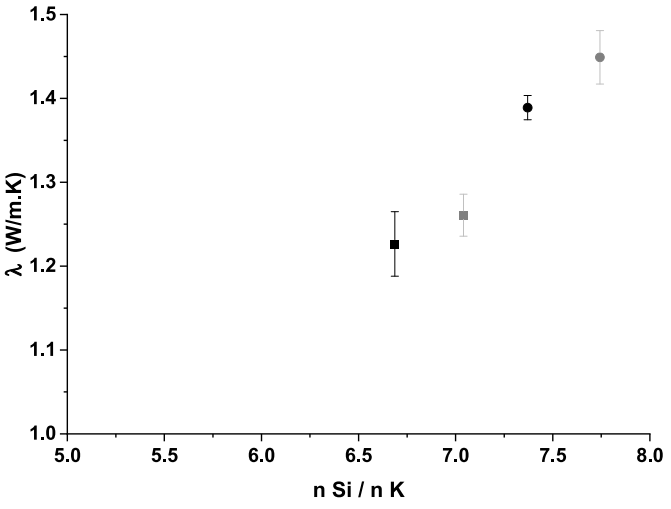


**Fig. 10.** Thermal conductivity as a function of the Si/K molar ratio for (■) $K^6M5S$, (▰) $K^6MSA$, (●) $K^5MS$, and (●)$K^5MSA$ samples.

Among the samples, two $K^6MS$ samples with different ages (40 and 28 days) are tested to evaluate the influences on the resistance and deformation. The sample has a high and repeatable deformation, differing from the sample with mullite the aluminosilicate additive ($K^6MSA$). During thermal shock (step 2), three compositions are tested: $K^6MS$, $K^6MSA$ and $K^5MSA$. The behaviors of the samples are different; the sample containing mullite $K^6MSA$ shows a strong deformation in a very

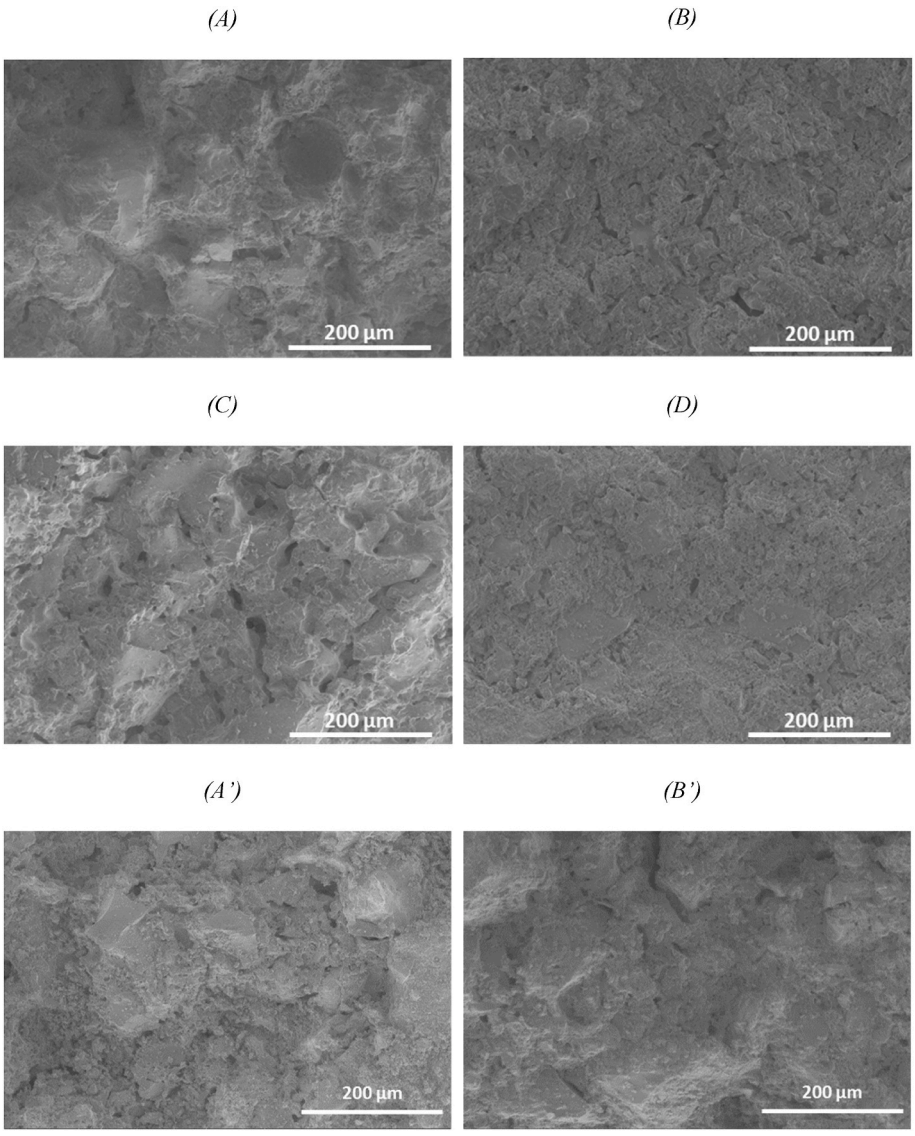


**Fig. 11.** SEM micrographs of (A) $K^6MS$, (B) $K^6MSA$, (C) $K^5MS$ and (D) $K^5MSA$ samples treated at 1000 °C in a laboratory furnace and (A′) $K^6MS$ and (B′) $K^6MSA$ samples treated at Efectis according to ISO 834-1 standard thermal program.

short time, contrary to the reference sample. However, during this test, a problem occurs. The creep monitoring gauges prevent the measurement of deformation on sample $K^5MSA$. The good performance with the fast temperature increase is an opportunity to use these specific materials for their excellent fire resistance and thermal protection abilities.

To verify this behavior, the evolution characteristics of the thermal conductivity values of the laboratory samples are plotted as functions of the Si/K molar ratios in the mixtures (Fig. 10). The thermal conductivity increases with the molar ratio Si/K. For the $K^6$ samples, the thermal conductivities are comprised between 1.23 and 1.26 W $m^{-1}$ $K^{-1}$. The change of solution leads to an increase the conductivity of 1.39 and 1.44 W $m^{-1}$. $K^{-1}$, and the Si/K molar ratios are 6.35 and 6.66 for the $K^5MS$ and $K^5MSA$ samples, respectively. The increases in thermal conductivity values can be explained by the composition, which may vary between $K^5$ and $K^6$, and by the decrease in porosity, as previously observed [39]. The porosity values are 33% and 29% for the $K^6$ and $K^5$ samples, respectively. Moreover, different works have shown that the addition of silicon promotes an increase in the thermal conductivity [40] and that the chemical composition governs the thermal conductivity. Several works [41] have reported that the highest coefficient of thermal conductivity for metakaolin-based geopolymer paste is 0.76 W/m. K; based on analytical models, the thermal conductivity value of the solid skeleton of the geopolymer samples evolves between 0.95 and 1.45 W/m. K [42]. Using this material for thermal insulation and fire resistance building applications may be of interest. In addition to the thermal conductivity measurements, the heat capacity (Cp) estimates, based on the rule of mixtures using data from Richet [43], are performed on the $K^5$ and $K^6$ solution-based samples. To compare the compositions, the value of molar heat capacity is determined at 20 °C. Samples with $K^6$ have higher values (322 J $mol^{-1}$. $K^{-1}$) than those with $K^5$ (313 J $mol^{-1}$ $K^{-1}$). This slight difference is due to the ratio of Si/K in the solution, which is greater for $K^5$. The addition of mullite, the aluminosilicate additive decreases the value of the molar heat capacity. This change is induced by the composition and, in particular, the contributions of Si and Al to the mixture. Even if a difference is observed between the molar heat capacities of $K^5$ and $K^6$, the values calculated in units of mass are very close (0.750 J $g^{-1}$ $K^{-1}$).

The SEM micrographs of different samples treated at 1000 °C in the laboratory and according to the ISO 834-1 standard program are presented in Fig. 11. The $K^6MS$ laboratory sample (A) presents a microstructure characteristic of the presence of viscous flow due to the melting of the amorphous phase surrounding the different crystalized

particles. The $K^5MS$ (C) sample presents the same microstructure with a low viscous flow that is relatively more diffuse. The use of a solution concentrated in [K] favors the formation of viscous flow and an amorphous phase. The addition of the aluminosilicate additive ($K^6MSA$ (B) and $K^5MSA$ (D)) produces a heterogeneous microstructure without changes. The formation of high-temperature phases, such as leucite and anorthite, and the formation of a viscous flow favors temperature resistance and improves the mechanical properties of the samples. For the $K^6MS$ and $K^6MSA$ samples, a similar structure is observed between the samples treated in the laboratory and in the standardized thermal program. The scale-up and thermal treatment do not influence the sample microstructure. As previously observed in the laboratory, the reference sample ($K^6MS$) presents significant viscous flow formation. In contrast, the aluminosilicate additive $K^6MSA$ delays the densification of the material and limits the formation of viscous flow.

## 4. Conclusion

In this study, the effects of two potassium silicate solutions on the strength and thermal resistance are evaluated. Moreover, the effects of the change in scale on the geopolymer formulations and the validation of the thermal resistance at large scales are established for the samples.

- The type of alkali silicate solution used results in different mechanical behaviors during the various treatments. However, approximately the same phases are observed. However, the presence of kalsilite between 1000 and 1100 °C is only observed for the $K^6$ solution.
- The mechanical behaviors depend on the formation of both high-temperature phases, such as leucite and anorthite, and a viscous flow-favored temperature resistance. Moreover, the differences in the reactivities of the solutions can influence the properties of the geopolymer. The more alkaline the condensed solution is, the higher the compressive strength.
- Validation by an industrial standardized test shows that when the temperature reaches 1200 °C in the furnace, the sample external surface is 400 °C, providing the best insulating properties. This result is confirmed by thermal conductivity measurements, which are governed by the chemical composition, especially the Si/K molar ratio.

No changes in properties are observed by scale transfer. The tests validated in the laboratory are good compromises to validate fire protection and flame-retardant materials.

## Declaration of interest

The authors declare that they have no known competing financial interests or personal relationships that could have appeared to influence the work reported in this paper.

## Acknowledgments

This project was supported by Aliénor transfert and the Nouvelle–Aquitaine region under an INIFUGE contract.

## Appendix A. Supplementary data

Supplementary data to this article can be found online at https://doi.org/10.1016/j.oceram.2023.100462.

## References

[1] Hua-Tay Lin, Hemrick James, Advanced and Refractory Ceramics for Energy Conversation and Efficiency, Wiley-American Ceramic Society, 2016.
[2] M. Tognonvi, S. Petlitckaia, A. Gharzouni, M. Fricheteau, N. Texier-Mandoki, S. Rossignol, et al., High-temperature, resistant, argillite-based, alkali-activated materials with improved post-thermal treatment mechanical strength, Clay Clay Miner. (2020), https://doi.org/10.1007/s42860-020-00067-9.
[3] S. Petlitckaia, A. Gharzouni, M. Tognonvi, N. Texier-Mandoki, S. Rossignol, et al., Effect of water on the thermal properties argillite-based geopolymers, J. Non-Cryst. Solids 541 (2020), 120073, https://doi.org/10.1016/j.jnoncrysol.2020.120073.
[4] Z. Baifa, G. Haozhe, Y. Peng, D. Liangliang, Z. Xuemin, et al., Novel acid-based geopolymer synthesized from nanosizd tubular halloysite: the role of recalcination temperature and phospohoric acid concentration, Cement Concr. Compos. 110 (2020), 103601, https://doi.org/10.1016/j.cemconcomp.2020.103601.
[5] A. Nikolov, H. Nugteren, I. Rostovsky, Optimization of geopolymers based on natural zolite clinoptilolite by calcination and use of aliminate activators, Construct. Build. Mater. 243 (2020), 118257, https://doi.org/10.1016/j.conbuildmat.2020.118257.
[6] V. Phavongkham, S. Wattanasiriwech, T.W. Cheng, D. Wattanasiriwech, Effects of surfactant on thermo-mechanical behavior of geopolymer foam paste made with sodium perborate foaming agent, Construct. Build. Mater. 243 (2020), 118282, https://doi.org/10.1016/j.conbuildmat.2020.118282.
[7] A.M. Rashad, A.A. Hassan, S.R. Zeedan, An investigation on alkali-activated Egyptian metakaolin pastes blended with quartz powder subjected to elevated temperatures, Appl. Clay Sci. 132–133 (2016) 366–376, https://doi.org/10.1016/j.clay.2016.07.002.
[8] P. Scanferla, A. Gharzouni, N. Texier-Mandoki, X. Bourbon, S. Rossignol, Effects of potassium-silicate, sands and carbonates concentrations on metakaolin-based geopolymers for high-temperature applications, Open Ceramics 10 (2022), 1000257, https://doi.org/10.1016/j.oceram.2022.100257.
[9] P. Duxson, G.C. Luckey, J.S.J. Van Deventer, The thermal evolution of metakaolin geopolymers : Part 2- Phase stability and structural development, J. Non-Cryst. Solids 353 (22–23) (2007) 2186–2200, https://doi.org/10.1016/j.jnoncrysol.2007.02.050.
[10] C. Dupuy, M. Fricheteau, M. Elie, A. Gharzouni, S. Rossignol, et al., Thermal resistance alkali-activated materials using argillite and two types of solution, Proceedings of the 42nd International Conference on Advanced Ceramics and Composites: Ceram. Eng. Sci. Proc. 39 (2019).
[11] Q. Yang, S. Zhang, S. Huang, Y. He, Effect of ground quartz sand on properties of high-strength concrete in the steam-autoclaved curing, Cement and Concerte research 30 (12) (2000) 1993–1998, https://doi.org/10.1016/S0008-8846(00)00395-1.
[12] I.A. Aksay, D.M. Dabbs, M. Sarikaya, Mullite for structural, electronic, and optical applications, J. Am. Ceram. Soc. 74 (1991) 2343–2358, https://doi.org/10.1111/j.1151-2916.1991.tb06768.x.
[13] P. Duxson, G.C. Lukey, J.S.J. Van Deventer, Thermal evolution of metakaolin geopolymers: Part1 – physical evolution, J of Non –Crystalline Solids 352 (52–54) (2006) 5541–5555, https://doi.org/10.1016/j.jnoncrysol.2006.09.019.
[14] J. Kohout, P. Koutník, P. Hájková, E. Kohoutová, A. Soukup, Effect of K/Al molar ratio on the thermos-mechanical properties of metakaolinite-based geopolymer composites, Polymers 13 (21) (2021), 13754, https://doi.org/10.3390/polym13213754.
[15] G. Christopoulou, F. Modarresifar, B.L. Allsopp, A.H. Jones, P.A. Bingham, Nonisothermal crystallization kinetics and stability of leucite and kalsilite from $K_2O$-$Al_2O_3$-$SiO_2$ glasses, J. Am. Ceram. Soc. (2018) 1–16, https://doi.org/10.1111/jace.15944.
[16] J. Archez, S. Maitenas, L. Demont, M. Charrier, R. Mesnil, S. Rossignol, et al., Strategy to shape, on half-meter scale, a geopolymer composite structure by additives manufacturing, Open Ceramics 5 (2021), 100071, https://doi.org/10.1016/j.oceram.2021.100071.
[17] G. La Scalia, M. Saeli, L. Adelfio, R. Micale, From lab to industry: scaling up green geopolymeric mortars manufacturing towards circular economy, J. Clean. Prod. 316 (2021), 128164, https://doi.org/10.1016/j.jclepro.2021.128164.
[18] D.A. Salas, A.D. Ramirez, N. Ulloa, H. Baykara, A.J. Boero, Life cycle assessment of geopolymer concrete, Construct. Build. Mater. 190 (2018) 170–177, https://doi.org/10.1016/j.conbuildmat.2018.09.123.
[19] L. Vidal, E. Joussein, J. Cornette, J. Sanz, I. Sobrados, S. Rossignol, et al., Controlling the reactivity of silicate solutions: a FTIR, Raman, and NMR study, Colloids Surf. A Physicochem. Eng. Asp. 503 (2016) 101–109, https://doi.org/10.1016/j.colsurfa.2016.05.039.
[20] S. Petlitckaia, A. Gharzouni, I.N. Vlasceanu, O. Tanto, I. Sobrados, S. Rossignol, et al., Effect of kaolin and argilite mixture on the dielectric properties of geopolymers, Open Ceramics 4 (2020), 100035, https://doi.org/10.1016/j.oceram.2020.100035.
[21] S.E. Gustafsson, Transient plane source techniques for thermal conductivity and thermal diffusivity measurements of solid materials, Rev. Sci. Instrum. 62 (3) (1991) 797–804, https://doi.org/10.1063/1.1142087.
[22] J. Archez, R. Farges, A. Gharzouni, S. Rossignol, Influence of the geopolymer formulation on the endogeneous shrinkage, Construct. Build. Mater. 298 (2021), 123813, https://doi.org/10.1016/j.conbuildmat.2021.123813.
[23] K. Parthiban, S. Sreekumaran, Sustainable development of ultra high performance concrete using geopolymer technology, J. Build. Eng. 39 (2021), 102267, https://doi.org/10.1016/j.jobe.2021.102267.
[24] M. Arnoult, C. Dupuy, M. Colas, J. Cornette, L. Duponchel, S. Rossignol, Determination of the reactivity degree of various alkaline solutions: a chemometric investigation, Appl. Spectrosc. 73 (12) (2019) 1361–1369, https://doi.org/10.1177/0003702819867956.
[25] P. Scanferla, A. Gharzouni, N. Texier-Mandoki, X. Bourbon, I. Sobrados de la Plaza, S. Rossignol, Polycondensation reaction effect on the thermal behavior of metakaolin-based potassium geopolymers, J. Sol. Gel Sci. Technol. (2023), https://doi.org/10.1007/s10971-023-06080-3.

[26] A. Gharzouni, I. Sobrados, E. Joussein, S. Baklouti, S. Rossignol, Predictive tools to control the structure and the properties of metakaolin based geopolymer materials, Colloids Surf. A Physicochem. Eng. Asp. 511 (2016) 212–221, https://doi.org/10.1016/j.colsurfa.2016.09.089.
[27] C. Dupuy, A. Gharzouni, N. Texier-Mandoki, X. Bourbon, S. Rossignol, Thermal resistance of argillite-based alkali-activated materials. Part 1: effect of calcination processes and alkali cation, Mater. Chem. Phys. 217 (2018) 323–333, https://doi.org/10.1016/j.matchemphys.2018.06.079.
[28] W.D. Kingery, Introduction to Ceramics, John Wiley and Sons, Inc, London, 1967. New York.
[29] J. Peyne, A. Gharzouni, I. Sobrados, S. Rossignol, Idenfiying the difference between clays used in the brick industry by varous methods : iron extraction and NMR spectroscopy, J. Applied Clay Science 160 (2018) 290–298, https://doi.org/10.1016/j.clay.2018.02.037.
[30] L. Nodari, E. Marcuz, L. Maritan, C. Mazzoli, U. Russo, Hematite nucleation and growth in the firing of carbonate-rich clay for pottery production, J. of Eur. Cram. Soc. 27 (2007) 4665–4673, https://doi.org/10.1016/j.jeurceramsoc.2007.03.031.
[31] P. Linus, S.B. Hendricks, The crystal structures of hematite and corundum, J. Am. Chem. Soc. 47 (1925) 781–790, https://doi.org/10.1021/ja01680a027.
[32] C. Weigel, C. McCammon, H. Keppler, High-temperature Mössbauer spectroscopy: a probe for the relaxation time of Fe species in silicate melt and glasses, Am. Mineral. 95 (2010) 1701–1707, https://doi.org/10.2138/am.2010.3490.
[33] S. Petlitckaia, A. Gharzouni, E. Hyvernaud, N. Taxier-Mandoki, X. Bourbon, S. Rossignol, Influence of the nature amount of carbonate additions on the thermal behaviour of geopolymers : a model for prediction of shrinkage, Construct. Build. Mater. 296 (2021), 123752, https://doi.org/10.1016/j.conbuildmat.2021.123752.
[34] P. Ptáček, T. Opravil, F. Šoukal, J. Havlica, R. Holešinský, Kinetics and mechanism of formation of gehlenite, Al-Si spinel and anorthite from the mixture of kaolinite and calcite, Solid State Sci. 26 (2013) 53–58, https://doi.org/10.1016/j.solidstatesciences.2013.09.014.
[35] A. Autef, E. Prud'homme, N. Essaidi, P. Michaud, B. Samet, S. Rossignol, et al., Defining existence domains in geopolymers through their physicochemical properties, Appl. Clay Sci. 73 (2013) 26–34, https://doi.org/10.1016/j.clay.2012.10.013.
[36] B.P. Bezerra, M.R. Morelli, A.P. Luz, Effect of reactive silica source on the properties of Na-metakaolin-based geopolymer binder, Construct. Build. Mater. 364 (2023), 129989, https://doi.org/10.1016/j.conbuildmat.2022.129989.
[37] P. Duxon, G.C. Lukey, J.S.J. Van Deventer, Evolution of gel structure during thermal processing of Na-geopolymer gels, Am. Chem. Soc. 22 (2006) 8750–8757, https://doi.org/10.1021/la0604026.
[38] X. Jiang, Y. Zhang, R. Xiao, P. Polaczyk, M. Zhang, W. Hu, et al., A comparative study on geopolymers synthesized by different classes of fly ash after exposure to elevated temperatures, J. Clean. Prod. (2020), https://doi.org/10.1016/j.jclepro.2020.122500.
[39] F. Junjie, Z. Ruigand, G. Lunlun, L. Ye, C. Wei, C. Xudong, Development of porous fly ash-based geopolymer with low thermal conductivity, Mater. Des. 65 (2015) 529–533, https://doi.org/10.1016/j.matdes.2014.09.024.
[40] C. Zhenya, C. Shuai, J. Zhizhong, C. Hao, S. Jialog, J. Ke, H. Qunying, H. Jihua, Effect of Si-coated diamond on the relative density and thermal conductivity of diamond/W composites prepared by SPS, Vacuum 209 (2022), 111728, https://doi.org/10.1016/j.vacuum.2022.111728.
[41] Y. Tzong-Ruey, C. Ta-Peng, C. Chun-Tao, L. Yuan-Kai, C. Bo-Tsun, Effects of activating solution and liquid/solid ratio on engineering properties of metakaolin-based geopolymer, Appl. Mech. Mater. 204–208 (2012) 4101–4104. https://doi.org/10.4028/www.scientific.net/AMM.204-208.410.
[42] J. Henon, A. Alzina, J. Absi, D.S. Smith, S. Rossignol, Analytical estimation of skeleton thermal conductivity of a geopolymer foam from thermal conductivity measurements, Eur. Phys. J. Spec. Top. 224 (2015) 1715–1723. https://doi-org.ezproxy.unilim.fr/10.1140/epjst/e2015-02493-8.
[43] P. Richet, Heat capacity of silicate glasses, Chem. Geol. 62 (1–2) (1987) 111–124, https://doi.org/10.1016/0009-2541(87)90062-3.